energies

MDPI

Article

Improvement in the Energy Autonomy and the Mechanical Performances of an Onboard Actuation Chain for Robotics

Abdoul-Aziz Ahmed Hassan [1,2,*], Abderrezzak Cherifi [2], Ouahid Bouchhida [3], Sebastien Charles [2] and Hassan Ali Barkad [1]

[1] Laboratoire de Recherche en Energie et Systèmes Énergétiques (LARESE), Université de Djibouti, Djibouti City 77401, Djibouti
[2] Laboratoire d'Ingénierie des Systèmes de Versailles, Université Paris Saclay, Université de Versaille Saint-Quentin (UVSQ), IUT Mantes en Yvelines, 78200 Paris, France; abderrezzak.cherifi@uvsq.fr (A.C.); sebastien.charles@uvsq.fr (S.C.)
[3] Laboratoire de Recherche en Electrotechnique et Automatique, Faculté de Technlogie, Université de Médéa, Aleger 26000, Algeria; bouchhida.ouahid@gmail.com
* Correspondence: abdoul-aziz_ahmed_hassan@univ.edu.dj

Abstract

This paper aims to improve the energy autonomy and the mechanical performances of an on-board drive chain for robotics. The energy autonomy improvement is performed by reducing electrical losses in the inverter. Electrical losses are reduced by decreasing the number of switching cycles per period of the inverter's power semiconductor switches, while maintaining a low Total Harmonic Distortion (THD). These improvements are expected thanks to a new control strategy called Pre-Calculated Pulse Width Modulation (PC PWM). The principle of this new control strategy is that all the symmetries of an ideal three-phase voltage system are assigned to the real output voltage of the inverter. Then the switching instants of the inverter's switches are determined off line, by means of Fourier's analysis, so that the maximum number of successive harmonics is zeroed. This allows the optimal switching sequence to be predefined, thereby reducing unnecessary commutations of the power switches. The performance of the new method (PC PWM) is evaluated through detailed simulation studies and compared with the conventional method called Sinusoidal Pulse Width Modulation (SPWM). The simulation results show that despite the reduction in the number of commutations per period, the performance of the actuation chain has been significantly improved with PC-PWM (new technique). Indeed, for the same mechanical load, the PC-PWM method allows for a lower current, a shorter transient response time and a lower torque ripple than the SPWM method.

Keywords: inverters; harmonics; Total Harmonic Distortion (THD); Sinusoidal Pulse Width Modulation (SPWM); Pre-Calculated PWM (PC-PWM); switching number; induction motor dynamics

Check for updates

Academic Editor: Ralph Kennel

Received: 8 April 2026
Revised: 30 April 2026
Accepted: 2 May 2026
Published: 7 May 2026

Copyright: © 2026 by the authors. Licensee MDPI, Basel, Switzerland. This article is an open access article distributed under the terms and conditions of the Creative Commons Attribution (CC BY) license.

1. Introduction

Nowadays, AC motors are widely used in industrial applications such as wind power generation systems [1], electrical traction [2], and high-performance industrial drives [3]. This widespread adoption is mainly due to their simple structure, robustness, low maintenance cost, compactness and lightness compared to DC motors [4]. Induction motors are low cost and offer good efficiency when their supply voltage profile is well suited [5]. DC-AC conversion is therefore crucial to optimize AC engine efficiency [6]. In addition,

the rapid development of high-power semiconductor devices with high switching capabilities, such as bipolar transistors, gate-turn-off thyristors, insulated gate bipolar transistors, and more recently, Silicon Carbide MOSFET, has enabled the development of various DC/AC inverter topologies including voltage source inverters (VSIs), current source inverters (CSIs), and Z-source inverters [7–10]. It well known that the power losses in the inverter are classified into two categories: conduction and commutation [7,11], and that conduction losses are negligible compared to switching losses [12,13]. When the switch is in its stable "on" state, the voltage between its terminals is zero; and when the switch is in its "off" state, the current flowing through it is zero. The power lost within the switch is then zero in both of the two stable states "on" and "off" [13]. In contrast, during the transient switching operation, the current and the voltage are simultaneously non-zero. Then each switching operation induces a non-zero power loss within the switch, during the transition of the switch's state when the voltage and the current are simultaneously non-zero [13]. The solution to reduce power losses is therefore to decrease the number of switching operations [7,12,14]. The power losses in the inverter are converted to heat, which risks damaging the semiconductor switch through overheating [15]. To avoid overheating, diffusers powered by small motors are used; this further increases power loss and size [15]. However, harmonics and high switching frequency remain major issues in power electronic converters and electric drive actuators. Excessive switching frequency increases switching losses and reduces the overall efficiency of the converter [7,12,14]. These harmonics have two detrimental impacts: mechanical and electrical. The mechanical impact manifests as torque ripples, causing rotor vibrations and thus accelerating wear on its guide bearings. The detrimental electrical impact leads to the appearance of a skin effect (increased resistance of conductors in a winding), eddy currents (currents induced in the conductive volume of the ferromagnetic core of the windings), and hysteresis (faster friction and orientation of Weiss domains). Consequently, Joule and ferromagnetic losses increase. To address these issues, several modulation techniques have been proposed, among which the most widely used are Sinusoidal Pulse Width Modulation (SPWM) and Selective Harmonic Elimination Pulse Width Modulation (SHE-PWM) [14,16]. The major difference between these two approaches lies in the way the switching angles are determined. In SPWM, the switching instants are generated online in real time by comparing a sinusoidal reference signal with a high-frequency triangular carrier. Although this technique is simple to implement, it usually requires a relatively high switching frequency. In contrast, in SHE-PWM, the switching angles are calculated offline by solving a system of transcendental nonlinear equations. This approach allows specific harmonics to be eliminated while operating at relatively low switching frequencies, which makes its implementation less computationally demanding during real-time operation [17]. Basically, the SHE-PWM technique involves two main steps. The first step consists of determining the optimal switching angles by solving nonlinear transcendental equations. These calculations are performed offline using different numerical approaches such as iterative methods, elimination theory, Walsh functions, or optimization techniques including genetic algorithms and particle swarm optimization [16,17]. In the second step, the calculated switching angles are stored in look-up tables and used during real-time operation to generate the switching signals [14]. Recently, several works such as [14,17] have proposed improved strategies for harmonic control in real-time applications. They introduced a modulation strategy based on a modified sinusoidal carrier that is compared with a sinusoidal reference rather than with a triangular carrier, as in conventional PWM methods. A generalized real-time harmonic control (RTHC) approach has also been reported in [14,17]. All these methods propose an increase in the number of commutations to improve the energy quality and reduce the THD. The dilemma is that the power switching losses increase [7,12,14].

In this paper, a new inverter control strategy referred to as the PC-PWM technique is proposed. In this approach, the switching instants of the inverter are determined offline through a pre-calculation process, allowing the optimal switching sequence to be predefined. This strategy aims to maximize the number of zeroed low successive rank harmonics and to minimize the number of commutations of semiconductor switches. The proposed method is applied to the control of a three-phase induction motor drive. Simulation results demonstrate that the proposed technique (PC-PWM) necessitates a low number of switching operations per period (30) compared to conventional SPWM (180), provides a fast speed response, and reduces torque ripple, which contributes to the protection against bearing wear when compared with the conventional SPWM control strategy.

This paper is organized in six sections. After the introduction, Section 2 describes the onboard actuation chain constitution. Section 3 gives the theoretical background of the proposed PC-PWM, especially the study of the symmetry properties of an ideal three-phase voltage system and the reconstruction of the actual inverter output voltages in a complete period from only the sixth period, by using symmetry properties of an ideal voltage system and the calculation of the commutation instants improving the actuation chain performances using Fourier analysis. Section 4 is devoted to the induction motor model. Comparative simulation results are given and discussed in Section 5. Finally, Section 6 concludes the paper by summarizing the main improvements of an onboard actuation chain.

2. The Onboard Actuation Chain Description

Figure 1 shows the actuation chain, which is composed from the batteries, the three-phase inverter (with its gate signal generation), the induction motor, the single-ratio reducer and the mechanical load.

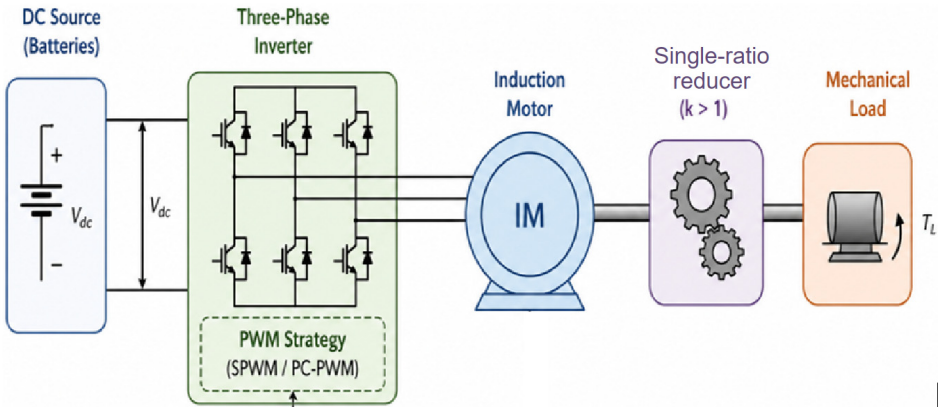


Figure 1. Onboard actuation chain.

The actuation chain consists of a mechanical part and an electrical part.

2.1. The Mechanical Part Description

The mechanical part of the drive chain consists of a single-ratio (k > 1) reducer and a mechanical load that the robot must lift. Unlike internal combustion engines powered by fossil fuels, a multi-speed gearbox is not necessary. This is because the variation in torque and speed can be more easily achieved by the electrical part [18–20]. The fact that a single-ratio reducer is sufficient allows for better rigidity of the mechanical assembly and a reduced footprint. The role of the single-ratio reducer is to amplify the electromagnetic torque generated by the electrical part (k > 1) [21]. This allows the motor to operate at low torque. Since torque is proportional to current, the motor can then operate at low current,

which reduces energy losses in the form of heat due to the Joule effect in the motor's copper windings [22,23]. This study focused on the electrical part.

2.2. The Electrical Part Description

The electrical part consists of a three-phase AC induction motor powered by a three-phase inverter itself fed by embedded batteries, where the output voltage is Vdc. The conversion from DC to three-phase AC voltage is performed by the three-phase inverter, as illustrated in Figure 1 [24,25]. The three-phase inverter topology used in this work is the conventional line-to-line three-level voltage, three-phase bridge inverter [25]. This one is composed of three legs connected in parallel across the DC-link (Vdc) [25]. Each leg contains two complementary power semiconductor switches associated with antiparallel diodes to allow bidirectional current flow required by inductive loads such as induction motors [26,27]. In each inverter leg, the two switches must be in a complementary state to prevent short-circuiting of the DC-link. Consequently, when the upper switch of a leg is turned ON, the lower switch must remain OFF, and vice versa. This complementary operation ensures safe switching and proper voltage synthesis at the inverter output [26,27]. The midpoints of the three inverter legs form the output terminals a, b, and c, which are connected to the stator windings of the three-phase induction motor [25].

The inverter generates the line-to-line voltages, which are applied to the machine and are defined as: U_{ab}, U_{bc} and U_{ca}. These voltages constitute a balanced three-phase voltage system used to drive the induction motor [25]. In the conventional method, the conversion from DC to AC is performed by means of Sinusoidal Pulse Width Modulation (SPWM) [28,29]. In this method, the switching times are determined in line by the intersection of the reference signal whose frequency is f and the triangular signal whose frequency is mf [28,29]. In the proposed method, the switching times are pre-calculated off-line (PC-PWM). Thanks to this proposed method, the performances of the drive chain are optimized. As a result, the proposed method allows a reduction in the switching number per period, in the switching losses, in the THD, and in torque ripple. Then the inverter can produce a high-quality three-phase voltage waveform suitable for the efficient operation of the induction motor. Then, the energy autonomy of the onboard actuator chain is increased and the bearing wear is decreased.

Figure 2 shows the ideal three phase voltage system. U with numerical indices (U_{12}, U_{23} and U_{31}) corresponds to the ideal voltages. U with alphabetical indices (U_{ab}, U_{bc} and U_{ca}) corresponds to the actual voltages in the inverter output.

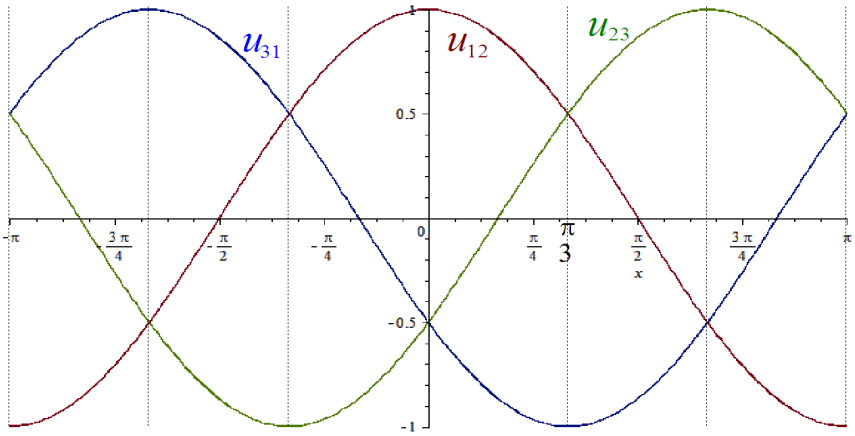


Figure 2. Three phase ideal voltage system.

3. Theoretical Background of the Proposed PC-PWM

3.1. The Principle of the Proposed PC-PWM

In order to improve the performance of the inverter and reduce switching losses, an innovative control strategy based on PC-PWM is adopted. Unlike conventional SPWM techniques, where the switching signals are generated by comparing reference and carrier signals, the proposed method determines the switching angles in advance using Fourier series analysis. The calculation model is based on the harmonic decomposition of the inverter output voltage. The sine and cosine Fourier coefficients are expressed as functions of the switching angles for a chosen number of commutations during one electrical period. The objective is to determine these angles such that the largest possible number of successive low-order harmonics are eliminated, starting from the lowest harmonic order (two). The PC-PWM method is based on the following principle: all symmetries and anti-symmetries of an ideal three-phase voltage system are attributed to the inverter output voltage.

3.2. Study of the Symmetry Properties of an Ideal Three-Phase Voltage System

The calculation of the switching angles is greatly simplified by exploiting all symmetries and anti-symmetries of an ideal three-phase voltage system. This one contains five symmetry properties, as shown in Figure 2, where u_{12}, u_{23} and u_{31} represent an ideal three-phase voltage system. These properties are attributed to the line-to-line output voltages of the reel inverter, namely U_{ab}, U_{bc}, and U_{ca}.

The five properties of symmetry and anti-symmetry of an ideal three-phase voltage system are:

1. U_{12} is an even function:

$$U_{12}(-\alpha) = U_{12}(\alpha) \tag{1}$$

2. U_{12} is anti-symmetric with respect to $\frac{\pi}{2}$:

$$U_{12}\left(\frac{\pi}{2} + \alpha\right) = -U_{12}\left(\frac{\pi}{2} - \alpha\right) \tag{2}$$

3. U_{23} is a symmetry of U_{12} with respect to $\frac{\pi}{3}$:

$$U_{23}\left(\frac{\pi}{3} + \alpha\right) = U_{12}\left(\frac{\pi}{3} - \alpha\right) \tag{3}$$

4. U_{31} is a shifted anti-symmetry of U_{12} with respect to $\frac{\pi}{3}$:

$$U_{31}\left(\frac{\pi}{3} - \alpha\right) = -U_{12}(\alpha) \tag{4}$$

5. The sum of the three line-to-line voltages is equal to zero:

$$U_{12}(\alpha) + U_{23}(\alpha) + U_{31}(\alpha) = 0 \tag{5}$$

It can be seen below that these symmetry and anti-symmetry properties significantly reduce the complexity of the Fourier series representation and allow the elimination of several harmonic components without explicitly solving additional equations.

3.3. Attribution of the Symmetry Properties of the Ideal Three-Phase Voltage System to the Actual Inverter and Fourier Analysis

In order to determine the harmonic content of the inverter output voltage and to establish the switching angle calculation model, the line-to-line voltage U_{ab} is decomposed in the Fourier series. The Fourier's coefficients of the voltage U_{12} are given by:

$$\begin{cases} a_k = \frac{1}{\pi}\int_{-\pi}^{\pi} u_{ab}(\alpha)\cos(k\alpha)\ d\alpha \\ b_k = \frac{1}{\pi}\int_{-\pi}^{\pi} u_{ab}(\alpha)\sin(k\alpha)\ d\alpha \end{cases} \quad (6)$$

By exploiting the symmetry properties of the inverter output voltage, the calculation of these coefficients can be significantly simplified. According to property 1, which indicates that the voltage waveform U_{ab} is an even function, the Fourier's sine coefficient becomes zero, and the cosine one becomes:

$$\begin{cases} a_k = \frac{2}{\pi}\int_{-\pi}^{\pi} u_{ab}(\alpha)\cos(k\alpha)\ d\alpha \\ b_k = 0 \end{cases} \quad (7)$$

Furthermore, by applying property 2, which indicates that the voltage U_{12} is anti-symmetric with respect to $\frac{\pi}{2}$, additional simplifications can be obtained. In this case, all cosine even harmonics have vanished. The remaining non-zero coefficients are only odd harmonics, as expressed in Equation (8) below:

$$\begin{cases} a_{k=2p+1} = \frac{4}{\pi}\int_{0}^{\pi} u_{ab}(\alpha)\cos(k\alpha)\ d\alpha \\ a_{k=2p} = 0 \\ b_k = 0 \end{cases} \quad (8)$$

To further simplify the calculation, the integration interval is decomposed into two subintervals:

$$\left[0, \frac{\pi}{2}\right] = \left[0, \frac{\pi}{3}\right] + \left[\frac{\pi}{3}, \frac{\pi}{2}\right] \quad (9)$$

By applying property 3 within the interval, performing a suitable change in variables, and using properties 4 and 5, which correspond to symmetry and anti-symmetry with respect to $\pi/3$, the Fourier coefficients can be rewritten as:

$$\begin{cases} a_{k=2p+1} = \frac{8}{\pi}\cos\left(k\frac{\pi}{6}\right)\int_{0}^{\frac{\pi}{3}} u_{ab}(\alpha)\cos\left[k\left(\alpha+\frac{\pi}{6}\right)\right]d\alpha \\ a_{k=2p} = 0 \\ b_k = 0 \end{cases} \quad (10)$$

From this formulation, it can be observed that the switching angles can be chosen only in the interval $\left[0, \frac{\pi}{3}\right]$ T. The remaining portions of the waveform can be reconstructed using the symmetry properties of an ideal three-phase system. The term $\cos(k\pi/6)$ indicates that all harmonics whose rank is a multiple of three are zero (k odd). Indeed:

$$\cos\left[3(2p+1)\frac{\pi}{6}\right] = \cos\left[(2p+1)\frac{\pi}{2}\right] = 0 \quad (11)$$

It can therefore be concluded that all harmonics whose rank is a multiple of 2 or 3 are already zeroed:

$$a_{k=2p} = a_{k=3p} = 0 \quad (12)$$

Consequently the rank of the remaining non-zero harmonics is odd and a non-multiple of three: $k = 6q \pm 1$, which corresponds to the ranks: 5, 7, 11, 13, 17, 19, ...

The Figure 3 below shows the zeroed and the remaining non-zero harmonics. This figure reveals that four out of six harmonics are zeroed, only by taking into account the

symmetrical properties of an ideal three-phase system. This relieves the inverter, which only has to cancel two harmonics out of each family of six harmonics.

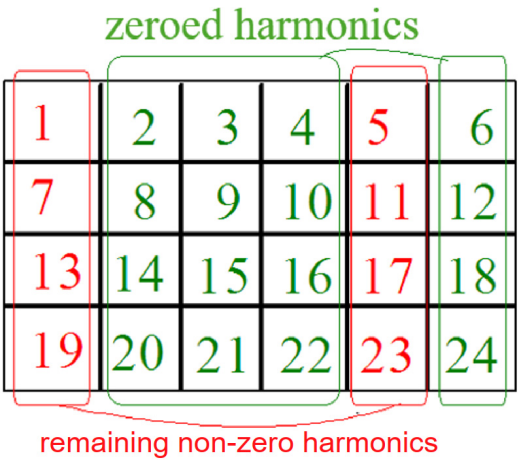


Figure 3. Symmetries: zeroed and remaining non-zero harmonics.

3.4. Reconstruction of the Output Voltages in a Complete Period

The DC-link voltage applied in the input of the inverter is generated by the onboard batteries (Vdc). This voltage feeds the three-phase inverter, which generates the AC voltage applied to the load. It can be seen in Equation (11) that the number of switching operations can be chosen only in the sixth of the period $\left[0, \frac{\pi}{3}\right]$. To reduce the number of switching operations per period, we have chosen only two commutations within one sixth of the electrical period: α_1 and α_2 with $0 < \alpha_1 < \alpha_2 < \pi/3$. The corresponding waveforms illustrating the switching instants are shown in the Figure 4 representing the inverter output voltage in one sixth of the period and in one third of the period: $[0, \frac{\pi}{3}]$.

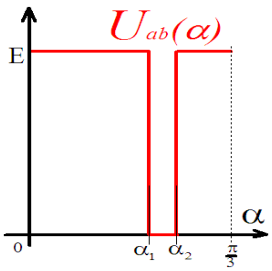


Figure 4. Chosen voltage waveform in sixth period $[0, \pi/3]$.

The Figure 4 above shows the chosen inverter output voltage U_{ab} in $[0, \pi/3]$. U_{ab} is assumed to have two commutations (α_1 and α_2). The complete waveform over the interval $[0, 2\pi]$ will be reconstructed from the voltage defined in $[0, \pi/3]$ by using the five symmetry properties discussed previously. U_{ca} will be deduced in $[0, \pi/3]$ by a shifted anti-symmetry of U_{ab} (4th symmetry property) and U_{bc} is deduced by the inversed addition of U_{ab} and U_{ca} (5th property), as shown in Figure 5 below.

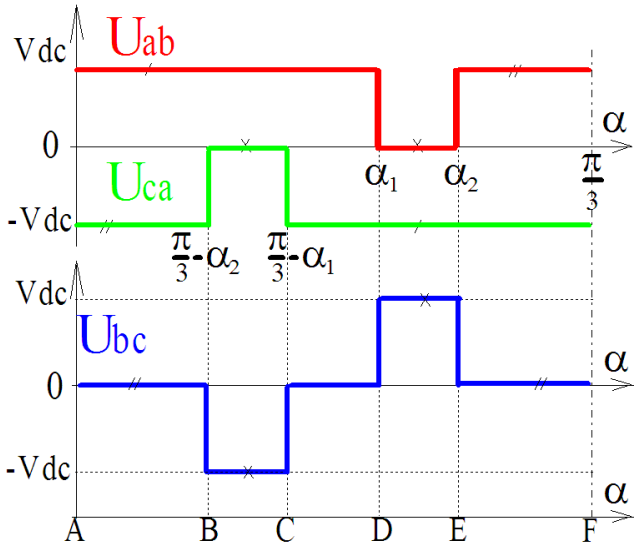


Figure 5. Deduction of U_{ca} and U_{bc} from U_{ab} in [0, π/3]. AB=p/3- a_2; BC=a_2-a_1; CD=2 a_1-p/3; DE=a_2-a_1; EF=p/3- a_2.

Figure 5 shows the construction of U_{ca} and U_{bc} from U_{ab} in the first sixth of the period (60°), according to the symmetry properties 4 and 5, respectively.

Figure 6 shows the construction of U_{ca} and U_{bc} from U_{ab} in the first half of the period (180°), according to the symmetry properties 4 and 5, respectively. Finally the reconstruction of the three-phase output voltages reveals that there are 30 commutations in a complete period $[0, 2\pi]$. Namely, 10 switching operations per phase and per period, as shown in Figure 7 below.

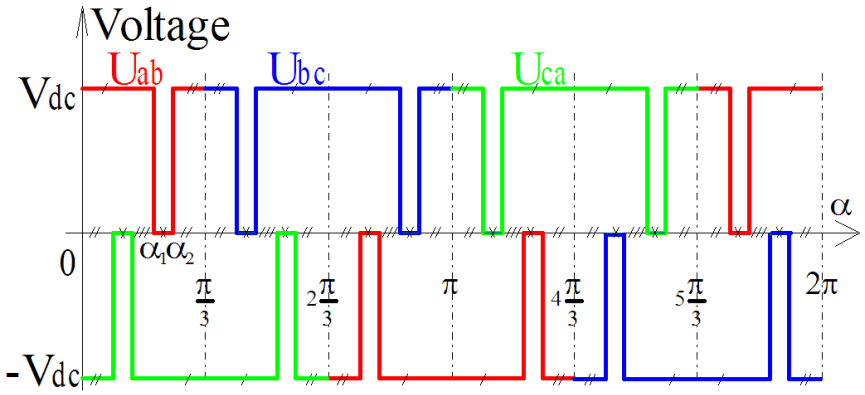


Figure 6. Reconstruction of the inverter output voltage in half period $[0, \pi]$.

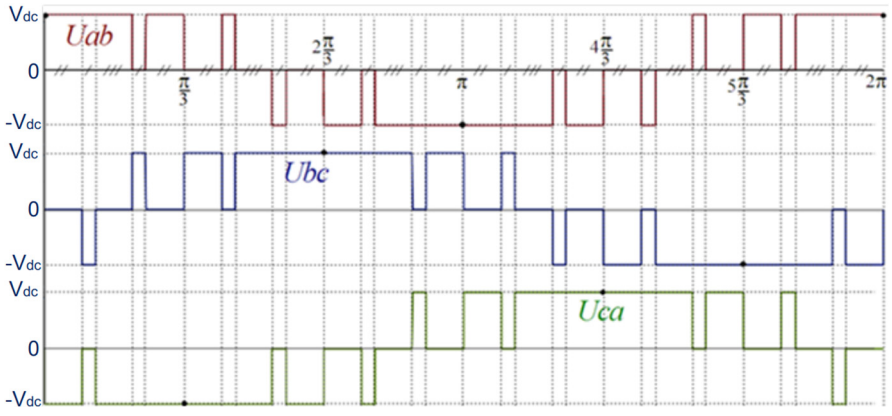


Figure 7. Reconstruction of output three phase voltages in one period.

3.5. Calculation of Switching Angles α_1 and α_2

Based on the Fourier analysis established previously, the coefficient corresponding to the odd harmonic order $k = 2p + 1$ is expressed as:

$$a_{k=2p+1} = \frac{8}{\pi}\cos\left(k\frac{\pi}{6}\right)\int_0^{\frac{\pi}{3}} u_{ab}(\alpha)\cos\left[k\left(\alpha+\frac{\pi}{6}\right)\right]\,d\alpha \tag{13}$$

Considering the piecewise expression of the voltage waveform in the interval, the integration interval is divided according to the switching instants α_1 and α_2. The voltage is equal to Vdc in the intervals [0, α_1] and it is equal to zero in the interval [α_1, α_2]. Consequently, the Fourier coefficient becomes:

$$a_{k=2p+1} = \frac{8E}{k\pi}\cos\left(k\frac{\pi}{6}\right)\left\{\sin\left[k\left(\alpha_1+\frac{\pi}{6}\right)\right] - \sin\left(k\frac{\pi}{6}\right) + \sin\left(k\frac{\pi}{2}\right) - \sin\left[k\left(\alpha_2+\frac{\pi}{6}\right)\right]\right\} \tag{14}$$

We can see in Equation (15) above that lower rank harmonics are of higher amplitude. Then the successive low-rank harmonics must be cancelled as a priority. Having only two adjustable variables ($\alpha_1 a$ and α_2), only two equations can be satisfied. Then we have chosen to eliminate the 5th and 7th harmonics. The corresponding Fourier equations are:

$$\begin{cases} a_5 = \frac{8}{5\pi}\cos\left(\frac{5\pi}{6}\right)E\left\{\sin\left[5\left(\alpha_1+\frac{\pi}{6}\right)\right] - \sin\left(\frac{5\pi}{6}\right) + \sin\left[5\left(\frac{\pi}{2}\right)\right] - \sin\left[5\left(\alpha_2+\frac{\pi}{6}\right)\right]\right\} = 0 \\ a_7 = \frac{8}{7\pi}\cos\left(\frac{7\pi}{6}\right)E\left\{\sin\left[7\left(\alpha_1+\frac{\pi}{6}\right)\right] - \sin\left(\frac{7\pi}{6}\right) + \sin\left[7\left(\frac{\pi}{2}\right)\right] - \sin\left[7\left(\alpha_2+\frac{\pi}{6}\right)\right]\right\} = 0 \end{cases} \tag{15}$$

These two equations form a system of nonlinear equations with two unknowns, $\alpha_1 a$ and α_2. This system was solved numerically using the simplex optimization method, which yields the following switching angles:

$$\begin{cases} \alpha_1 = 0.6620286986 \\ \alpha_2 = 0.7636303773 \end{cases} \tag{16}$$

Once these switching angles are determined, the inverter output voltage waveform over the entire electrical period [0, 2π] can be reconstructed using the symmetry properties of the three-phase system, as shown above. The resulting waveform provides a reduced switching frequency and eliminates the dominant low-order harmonics. The reconstructed three-phase voltage waveforms over the full electrical period are presented in Figure 7 above.

4. Induction Motor Model

In order to validate the performance of the proposed power conversion system, the dynamic model of the induction motor is implemented in the synchronous "d-q" reference frame [30–33]. This reference frame allows the three-phase variables to be transformed into two orthogonal components, which simplifies the mathematical representation of the machine and facilitates numerical simulation in Matlab/Simulink R2024b [34,35].The electrical dynamics of the induction machine are described by the following differential equations expressed in the synchronous d-q frame [32,33]:

$$\begin{cases} \frac{di_{ds}}{dt} = -\frac{1}{\sigma L_s}\left(R_s + R_r\frac{M_{sr}^2}{L_r^2}\right)i_{ds} + \omega_s i_{qs} + \frac{M_{sr}R_r}{\sigma L_s L_r^2}\psi_{dr} + \frac{M_{sr}}{\sigma L_s L_r}\psi_{qr}\omega_r + \frac{1}{\sigma L_s}V_{ds} \\ \frac{di_{qs}}{dt} = -\omega_s i_{ds} - \frac{1}{\sigma L_s}\left(R_s + R_r\frac{M_{sr}^2}{L_r^2}\right)i_{qs} - \frac{M_{sr}}{\sigma L_s L_r}\psi_{dr}\omega_r + \frac{M_{sr}R_r}{\sigma L_s L_r^2}\psi_{qr} + \frac{1}{\sigma L_s}V_{qs} \\ \frac{d\psi_{dr}}{dt} = \frac{M_{sr}R_r}{L_r}i_{ds} - \frac{R_r}{L_r}\psi_{dr} + \omega_g\psi_{qr} \\ \frac{d\psi_{qr}}{dt} = \frac{M_{sr}R_r}{L_r}i_{qs} - \omega_g\psi_{dr} - \frac{R_r}{L_r}\psi_{qr} \end{cases} \quad (17)$$

where the stator currents i_{ds} and i_{qs}, and the rotor flux linkages ψ_{dr} and ψ_{qr}, represent the electrical state variables of the machine. V_{ds} and V_{qs} represent d-axis and q-axis stator voltages. The mechanical dynamics of the rotor are governed by the motion equation.

$$\frac{d\Omega_r}{dt} = -\frac{f}{J}\Omega_r - \frac{1}{J}(C_{em} - C_r) \quad (18)$$

where J represents the rotor inertia and *f* is the viscous friction coefficient. The relationship between the electrical rotor speed ω_r and the mechanical rotor speed Ω_r is given by:

$$\Omega_r = \frac{\omega_r}{p} \quad (19)$$

where p denotes the number of pole pairs of the machine. The electromagnetic torque produced by the motor is expressed as:

$$C_{em} = p\frac{M_{sr}}{L_r}\left(\psi_{dr}i_{qs} - \psi_{qr}i_{ds}\right) \quad (20)$$

The slip angular speed ω_g appearing in the rotor flux equations is defined as:

$$\omega_g = \omega_s - \omega_r \quad (21)$$

where ω_s and ω_r represent the stator and rotor electrical angular speeds, respectively. The parameter σ denotes the leakage coefficient of the machine and is defined as:

$$\sigma = 1 - \frac{M_{sr}^2}{L_s L_r} \quad (22)$$

In these equations, *Rs* and *Rr* correspond to the stator and rotor resistances, *Ls* and *Lr* are the stator and rotor inductances, and *Msr* represents the mutual inductance between the stator and rotor windings.

5. Comparative Simulation Results and Discussion

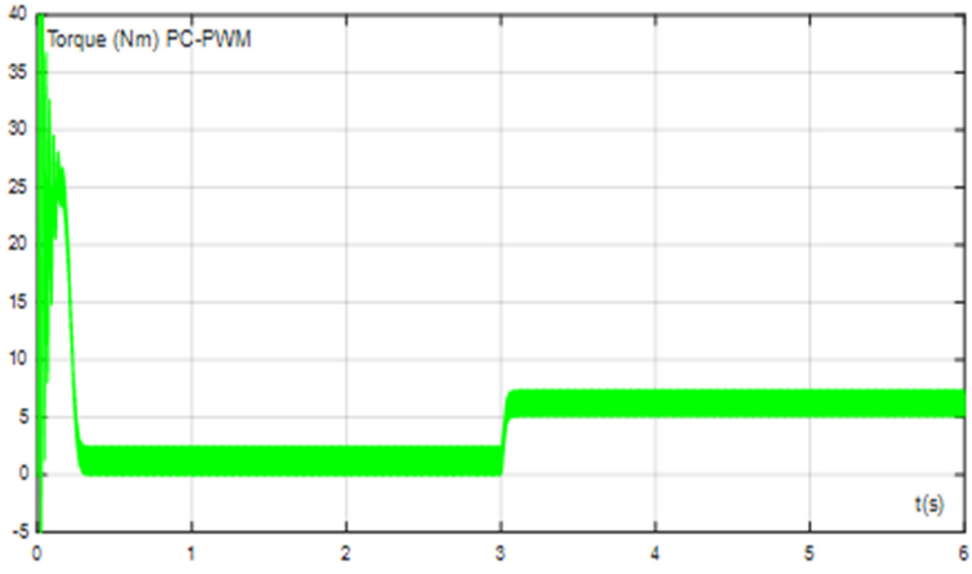
To evaluate the effectiveness of the proposed control strategy, detailed simulations were carried out using Matlab/Simulink for a three-phase squirrel-cage induction motor supplied by the proposed multilevel chopper–inverter structure. Two inverter modulation techniques were considered in the study: the conventional sinus–triangle PWM (SPWM) and the proposed PC-PWM strategy based on selective harmonic elimination [14,29,36]. The parameters of the induction motor used in the simulations correspond to a 1.5 kW squirrel-cage induction machine, whose main characteristics are summarized as follows in the Table 1:

Table 1. Parameters of the induction motor.

Symbol	Quantity	Value
P_n	Rate power	1.5 KW
V_n	Rate line voltage	220/380 V
C_n	Rated load torque	10 Nm
P	Poles pairs	2
R_s	Stator resistance	4.85 Ω
R_r	Rotor resistance	3.805 Ω
M_{sr}	Mutual inductance	0.258 H
L_s	Stator inductance	0.274 H
L_r	Rotor inductance	0.274 H
I_n	Rated current	6.4/3.7 A
Ω_n	Motor speed	1420 rpm
f	Viscosity coefficient	0.001136 N.m.s/rd
J	Inertia	0.031 kg.m^2

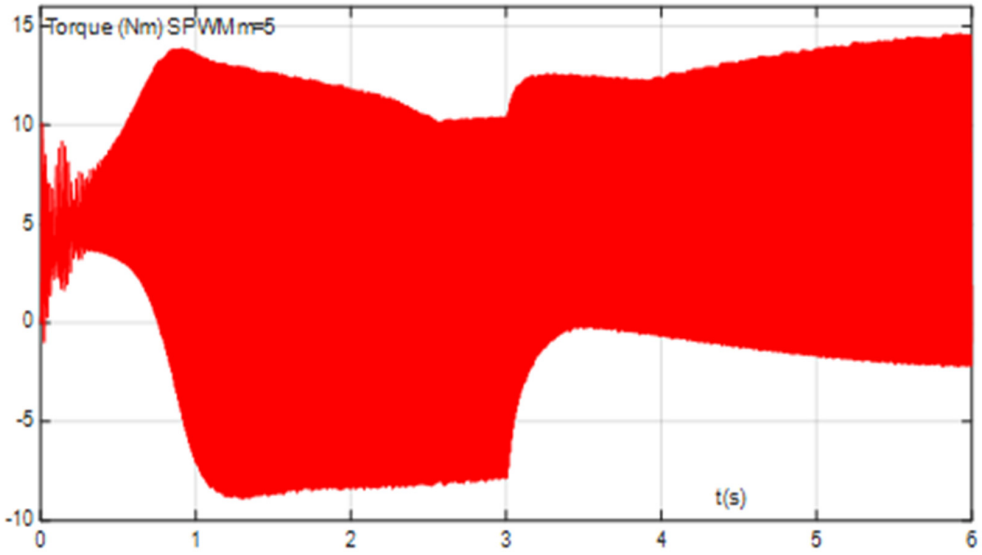
These parameters were implemented in the dynamic d-q model of the induction machine developed in Matlab/Simulink in order to analyze the behavior of the motor when supplied by the proposed inverter [36]. For the comparison to be relevant, the number of switching operations must be identical. We chose m = 5, which corresponds to 10 switching operations per phase per period. The impact of m was also studied (m = 5 and m = 31) for the same conditions. At the instant t = 3 s, a load torque of 5 Nm is applied to the motor in order to test the dynamic response of the drive system.

Figure 8a,b show the electromagnetic torque response of the induction motor, with the proposed PC-PWM and SPWM with m = 5, respectively. These figures correspond to the same number of switching operations per period and per phase: 10.



(**a**)

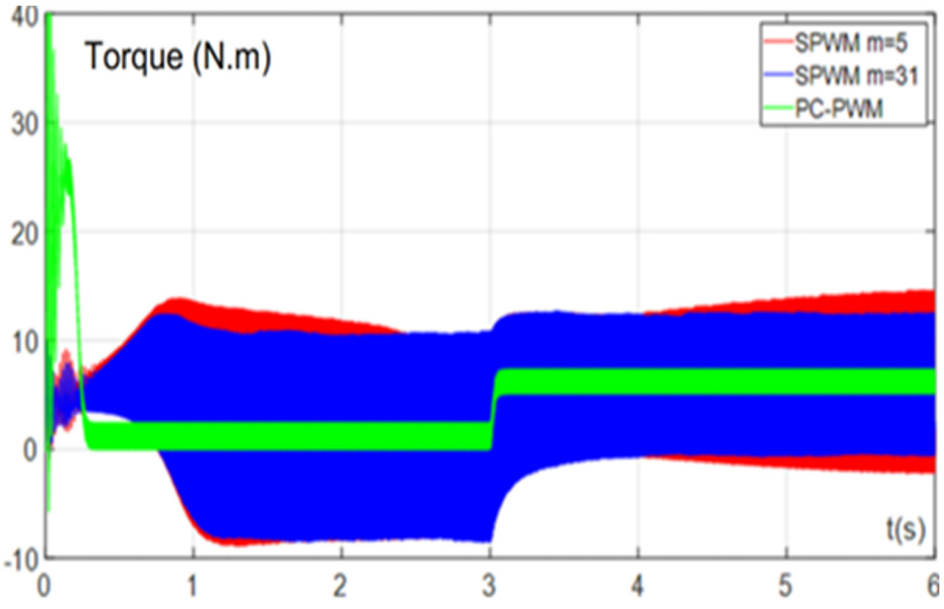
Figure 8. *Cont.*



(**b**)

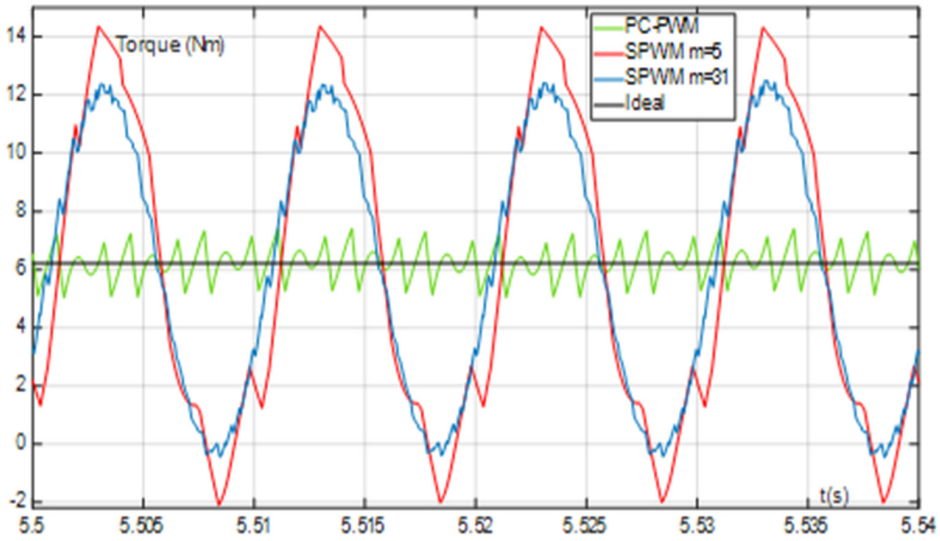
Figure 8. Electromagnetic torque of the induction motor. (**a**): With proposed PC-PWM; (**b**): with conventional SPWM, with m = 5.

Figure 9a,b show the comparison of the electromagnetic torque with PC-PWM, and SPWM with m = 5 and m = 31, in a large time interval ([0, 6 s]) and with zoom in permanent mode ([5.5, 5.54 s]). It can be seen in Figure 9 that the minimum torque ripple is obtained with the proposed PC-PWM method. It can be also observed that the impact of m is not significant. Indeed the augmentation of m from 5 to 31 engenders just a little reduction in torque oscillations. It can be noticed in Figures 8 and 9 that the PC-PWM's starting torque (transient mode) is higher and its torque ripple in permanent mode is significantly lower (3.5 times smaller) compared to the conventional SPWM. The reduction in the torque ripple will generate less vibration, which helps protect the guide bearings from wear and reduces audible noise. This improvement is mainly due to the selective elimination of successive low-ranked harmonics and the optimized switching angles used in the proposed PC-PWM strategy.



(**a**)

Figure 9. *Cont.*

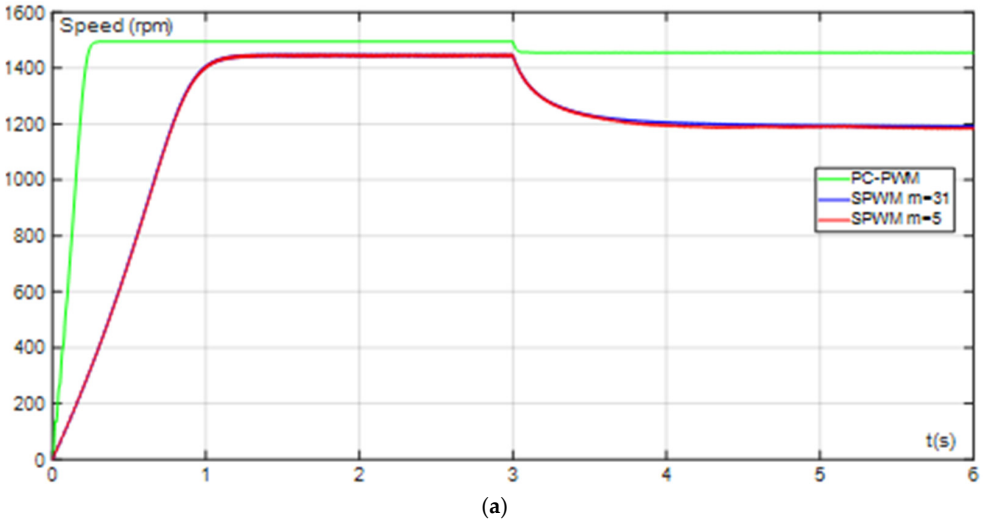


(**b**)

Figure 9. Electromagnetic torque with PC-PWM, SPWM m = 5 and SPWM m = 31. (**a**): In a large time interval ([0, 6 s]); (**b**): zoom in permanent mode ([5.5, 5.54 s]).

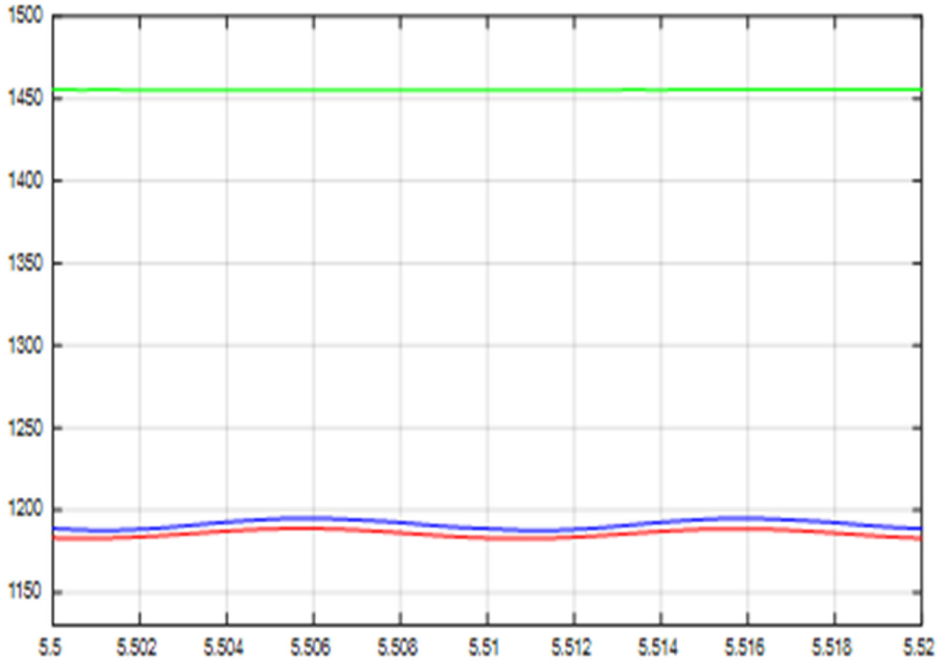
Figure 10a,b show the motor speed obtained with PC-PWM and SPWM-m = 31 and SPWM-m = 5. Here too, the proposed PC-PWM method generates better motor behavior: a more stable and higher speed in the permanent mode and a shorter transient mode. This observation holds true both before and after the introduction of the torque load of 5 N.m (at t = 3 s), demonstrating an improvement in dynamic performance, thanks to the proposed PC-PWM method.

Figure 11a–c present the stator phase current i_a of the induction motor, with SPWM m = 5, SPWM-m = 31 and PC-PWM, respectively, in a large time interval ([0, 6 s]). Figure 11d shows the comparison of this current after the establishment of the permanent mode. This figure clearly shows that the current amplitude obtained with PC-PWM is 2.5 times lower than that obtained with conventional SPWM. The Joule effect power lost due to PC-PWM is then 6.25 (2.5^2) times smaller than that of SPWM for the same mechanical power developed by the motor. The energy autonomy is then optimized with PC-PWM. The SPWM current has a slight delay compared to that of PC-PWM. This suggests a higher reactive power, of an inductive type, for SPWM.



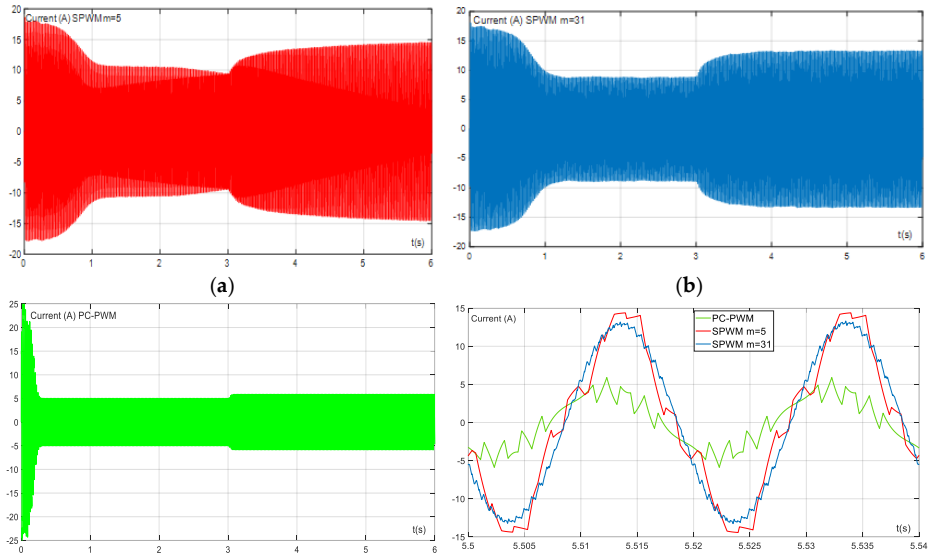
(**a**)

Figure 10. *Cont.*



(**b**)

Figure 10. Comparison of speed motor. (**a**): In a large time interval ([0, 6 s]); (**b**): zoom in permanent mode ([5.5, 5.54 s]).



(**a**) (**b**)

(**c**) (**d**)

Figure 11. Stator phase current i_a in the induction motor. (**a**) SPWM with m = 5; (**b**) WPWM with m = 31; (**c**) PC-PWM; (**d**) zoom in 40 mS of stator current, during permanent mode, with PC-PWM and SPWM (m = 5 and m = 31).

Figure 12 shows the stator phase current i_a for PC-PWM and for SPWM with m = 5 and m = 31. The comparison reveals that PC-PWM requires a lower current during a steady state, but a higher current during a transient state, for the same load. The PC-PWM strategy is smoother and exhibits lower harmonic distortion, which helps to reduce Joule effect losses in copper, and to improve the overall efficiency of the actuation chain.

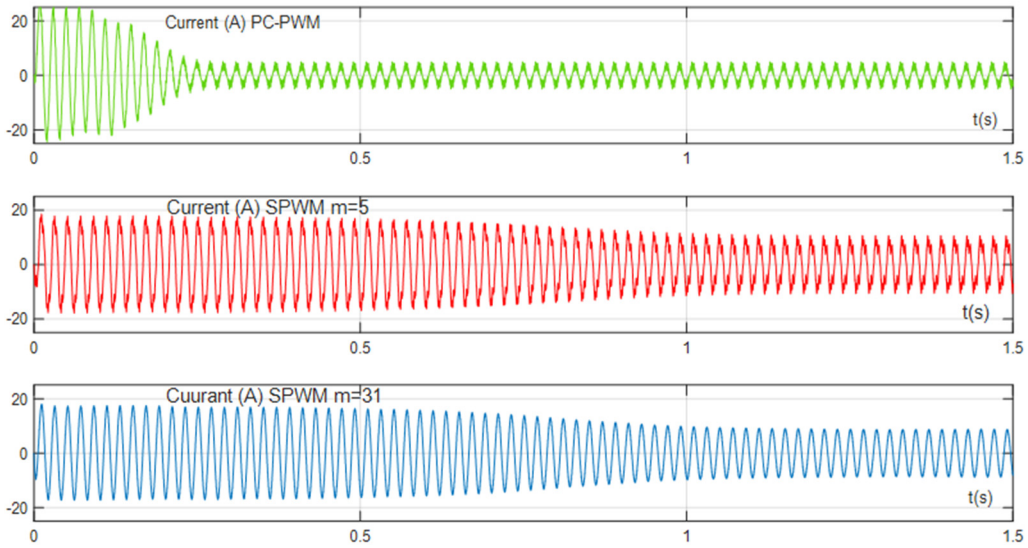


Figure 12. Comparison of the stator current using conventional SPWM and PC-PWM.

Figures 13 and 14 show the power semiconductor switch drain-source voltage (Vds) and the line-to-line inverter output voltage (Uab), respectively, for the proposed PC-PWM (a), the conventional SPWM-m = 5 (b), and SPWM-m = 31, during one period (20 ms). Figures (a) and (b) are for the same number of commutation operations (10 per period and per phase). Figure (c) is for 62 commutations per period and per phase. The conventional SPWM exhibits less symmetry than the proposed PC-PWM method.

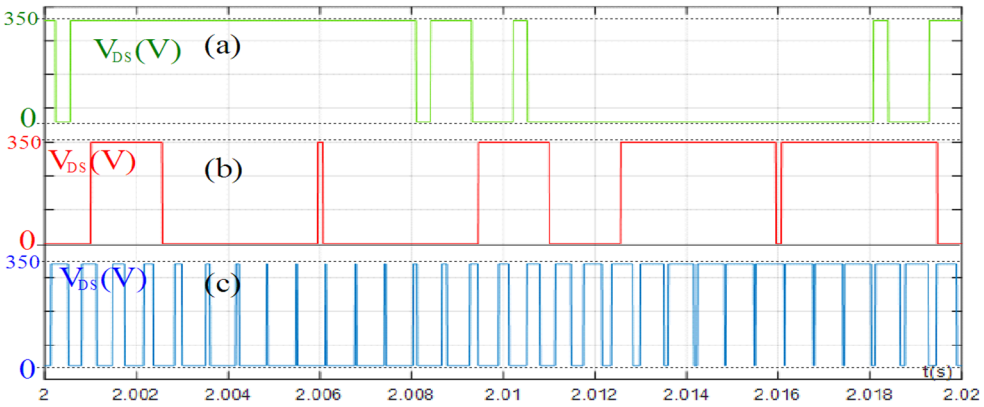


Figure 13. Voltage between the drain-source of a power semiconductor switch. (**a**): With the proposed PC-PWM; (**b**) with conventional SPWM-m = 5; (**c**): with conventional SPWM-m = 31.

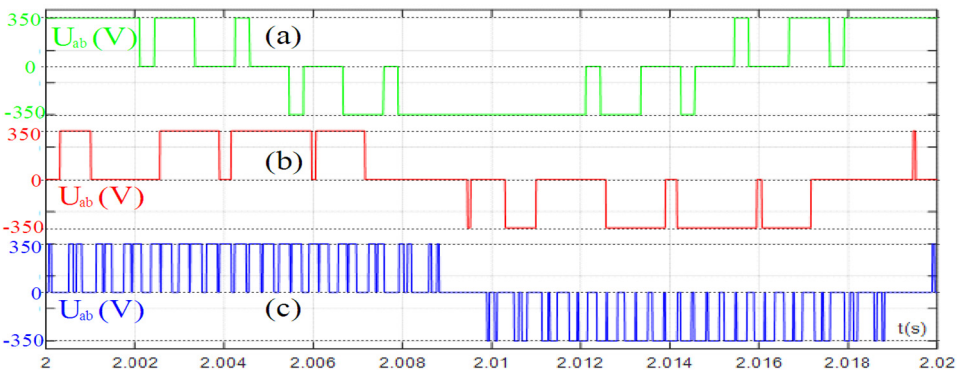


Figure 14. Inverter line-to-line output voltage. (**a**): With the proposed PC-PWM; (**b**) with conventional SPWM-m = 5; (**c**): with conventional SPWM-m = 31.

The results clearly show that, for the same number of switching operations per period and the same load torque, the PC-PWM strategy significantly reduces the harmonic distortion, the motor current and the torque ripple. This reduction leads to lower Joule effect power losses in the induction motor, lower mechanical vibrations in the actuation chain, less noise disturbance and protects the rotor guide bearings from wear.

Figure 15 shows the comparison between the proposed PC-PWM and the conventional method with m = 5 and m = 31, in terms of the harmonic spectrum. The Total Harmonic Distortion (THD) is shown in Table 2. It can be seen from the harmonic spectrum that the proposed PC-PWM method cancels all harmonics from two to 10. In contrast, the SPWM with (m = 5) presents high amplitudes in these harmonics. Increasing the modulation index to (m = 31) leads to a reduction in these components, but they still remain higher than those obtained with PC-PWM. This behavior is confirmed by the THD results. The lowest THD is obtained with the proposed PC-PWM (50.77%), while higher values are observed with SPWM (77.30% for (m = 5) and 73.37% for (m = 31)). It can also be noticed that increasing (m) improves the waveform quality, but the improvement remains limited compared to the proposed method. Finally, the cancellation of low-order harmonics leads to lower torque ripple, which helps reduce mechanical vibrations, limits wear of the bearings and decreases acoustic noise. This improvement is mainly due to the selective elimination of low-order harmonics and the optimized switching angles used in the PC-PWM strategy.

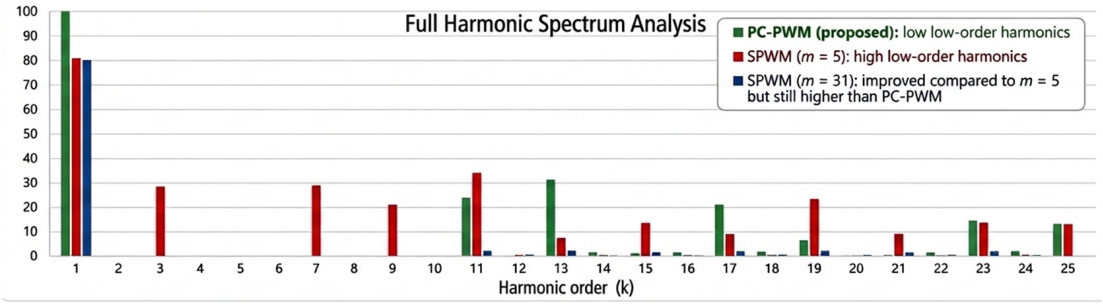


Figure 15. Harmonic analysis comparison for PC-PWM and SPWM.

Table 2. Total Harmonic Distortion (THD).

Method	PC-PWM	SPWM—m = 5	SPWM—m = 31
Fundamental (V)	308.9	250.4	248
THD (%)	50.77%	77.30	73.37

6. Conclusions

An innovative Pre-Calculated PWM (PC-PWM) strategy, based on symmetry in the properties of an ideal three-phase voltage system and on Fourier's analysis, was developed to minimize the number of switching operations and to maximize the number of zeroed harmonics. All the symmetry properties of an ideal three-phase voltage system were attributed to the reel inverter output voltages. Thanks to symmetry properties attribution, four out of each family of six harmonics are already zeroed. This reduces the constraint on the total number of commutations of the inverter's power semiconductor switches, which now only have to cancel two harmonics in each family of six harmonics. Indeed, with only 10 switching cycles per period of a three-level phase-to-phase voltage inverter, the first nine harmonics are successively canceled from two to 10: the rank of the first non-zero harmonic is 11. The performances of conventional SPWM and the proposed PC-PWM methods were compared using the d–q model of a squirrel-cage induction motor implemented in Matlab/Simulink, for the same conditions (same number of switching operations and same

mechanical load). The obtained comparative simulation results clearly demonstrate that the proposed PC-PWM method improves significantly the dynamic behavior of the actuation chain. In particular with the proposed PC-PWM, the rotor speed is higher and is stable after a lower transient time. The electromagnetic couple exhibits a lower ripple in both modes (transient and steady state). The stator current is lower for the same mechanical load. For the same number of switching operations (10 per period and per phase), the rotor speed is 20% higher, the torque ripple is 3.5 times lower and the stator current is 2.5 times lower than that of conventional SPWM. The Joule effect power lost due to PC-PWM is then 6.25 (2.5^2) times smaller than that of SPWM. Therefore, the proposed PC-PWM represents an effective solution for low-cost and high-performance robotics onboard actuation chains. The proposed PC-PWM improves the battery's autonomy, increases the energy efficiency of the actuation chain, reduces energy losses due to the Joule effect, decreases torque ripple, reduces vibration and noise, and protects the rotor guide bearings from wear. Future work may focus on the experimental validation of the proposed control strategy.

Author Contributions: A.-A.A.H. and A.C. conceived the study, developed the proposed methodology, performed the comparative simulations, discussed the data analysis, validated the simulation results, and wrote the original draft of the manuscript. O.B., S.C. and H.A.B. contributed to the implementation of the models, supervised the work, contributed to the scientific discussion, reviewed the manuscript, and gave a critical revision of the manuscript. All authors have read and agreed to the published version of the manuscript.

Funding: This research received no external funding.

Institutional Review Board Statement: Not applicable.

Informed Consent Statement: Not applicable.

Data Availability Statement: The data presented in this study are available on request from the corresponding author.

Conflicts of Interest: The authors declare no conflicts of interest.

Abbreviations

The following abbreviations are used in this manuscript:

PWM	Pulse Width Modulation
SPWM	Sinusoidal Pulse Width Modulation
PC-PWM	Pre-Calculated Pulse Width Modulation
AC/DC	Alternating Current/Direct Current

References

1. Chen, H.; Zuo, Y.; Chau, K.T.; Zhao, W.; Lee, C.H.T. Modern electric machines and drives for wind power generation: A review of opportunities and challenges. *IET Renew. Power Gener.* **2021**, *15*, 1864–1887. [CrossRef]
2. Paul, S.; Han, P.-W.; Chang, J.; Chun, Y.-D.; Lee, J.-G. State-of-the-art review of railway traction motors for distributed traction considering South Korean high-speed railway. *Energy Rep.* **2022**, *8*, 14623–14642. [CrossRef]
3. Azab, M. A Review of Recent Trends in High-Efficiency Induction Motor Drives. *Vehicles* **2025**, *7*, 15. [CrossRef]
4. Ameen, H.F.; Hamad, H.A.; Rasool, A.A. Performance Evaluation of Different NEMA Induction Motor Designs under the Effect of Unbalanced Supply Voltages. *Tikrit J. Eng. Sci.* **2024**, *31*, 158–171. [CrossRef]
5. Nasir, B.A. Determination of the Harmonic Losses in an Induction Motor Fed by an Inverter. *Eng. Technol. Appl. Sci. Res.* **2022**, *12*, 9536–9545. [CrossRef]
6. Caruso, M.; Di Tommaso, A.; Miceli, R.; Nevoloso, C.; Spataro, C. Uncertainty evaluation in the differential measurements of power losses in a power drive system. *Measurement* **2021**, *183*, 109795. [CrossRef]
7. Suthar, A.N.; Venkataramanaiah, J.; Suresh, Y. Conventional, wide-bandgap, and hybrid power converters: A comprehensive review. *Renew. Sustain. Energy Rev.* **2025**, *213*, 115419. [CrossRef]

8. Danapour, N.; Akbari, E.; Tarafdar-Hagh, M. A Review on the Power Circuit Topologies of Current Source Inverters in Photovoltaic Applications. *Iran. J. Electr. Electron. Eng.* **2022**, *18*, 2404. [CrossRef]
9. Subhani, N.; Kannan, R.; Mahmud, A.; Blaabjerg, F. Z-source inverter topologies with switched Z-impedance networks: A review. *IET Power Electron.* **2021**, *14*, 727–750. [CrossRef]
10. Shi, B.; Ramones, A.I.; Liu, Y.; Wang, H.; Li, Y.; Pischinger, S.; Andert, J. A review of silicon carbide MOSFETs in electrified vehicles: Application, challenges, and future development. *IET Power Electron.* **2023**, *16*, 2103–2120. [CrossRef]
11. Donuk, H. A New Soft-Switching Control Technique and Loss Analysis for Parallel Resonant DC-Link Inverter Connected to the Grid. *Tech. Gaz.* **2022**, *29*, 1576–1584. [CrossRef]
12. Zygmanowski, M.; Bodora, A.; Domoracki, A.; Frania, K.; Hetmańczyk, J.; Jarek, G.; Jeleń, M.; Kaczmarczyk, Z.; Kasprzak, M.; Lasek, P.; et al. Power Losses of the High-Voltage High-Frequency Coaxial Cable Energy Transfer System. *Electronics* **2025**, *15*, 93. [CrossRef]
13. Kinyua, J.M.; Aoki, M. SiC MOSFET Switching Dynamics and Power Conversion Loss Characterization Under Parametric Variations. *Energies* **2025**, *18*, 6264. [CrossRef]
14. Ali, M.; Al-Ismail, F.S.; Gulzar, M.M.; Khalid, M. A review on harmonic elimination and mitigation techniques in power converter based systems. *Electr. Power Syst. Res.* **2024**, *234*, 110573. [CrossRef]
15. Han, S.; Choi, H.; Jo, I.; Lee, H. Design optimization and performance evaluation of an air-cooled heat exchanger for electric vehicle power electronics cooling. *Appl. Therm. Eng.* **2026**, *283*, 128842. [CrossRef]
16. Pu, H.; Bai, Z.; Xin, Y.; Zhao, J.; Bai, R.; Luo, J.; Yi, J. Efficient (2N+1) selective harmonic elimination in modular multilevel converters using an evolutionary many-tasking approach with prior knowledge. *Appl. Soft Comput.* **2023**, *144*, 110468. [CrossRef]
17. Patangia, H.; Gourisetti, S.N.G. Real time harmonic elimination using a modified carrier. In *Proceedings of the CONIELECOMP 2012, 22nd International Conference on Electrical Communications and Computers, Cholula, Mexico, 27–29 February 2012*; IEEE: Piscataway, NJ, USA, 2012; pp. 273–277. [CrossRef]
18. Fang, S.; Song, J.; Song, H.; Tai, Y.; Li, F.; Nguyen, T.S. Design and control of a novel two-speed Uninterrupted Mechanical Transmission for electric vehicles. *Mech. Syst. Signal Process.* **2016**, *75*, 473–493. [CrossRef]
19. Gao, B.; Meng, D.; Shi, W.; Cai, W.; Dong, S.; Zhang, Y.; Chen, H. Topology optimization and the evolution trends of two-speed transmission of EVs. *Renew. Sustain. Energy Rev.* **2022**, *161*, 112390. [CrossRef]
20. Spanoudakis, P.; Moschopoulos, G.; Stefanoulis, T.; Sarantinoudis, N.; Papadokokolakis, E.; Ioannou, I.; Piperidis, S.; Doitsidis, L.; Tsourveloudis, N.C. Efficient Gear Ratio Selection of a Single-Speed Drivetrain for Improved Electric Vehicle Energy Consumption. *Sustainability* **2020**, *12*, 9254. [CrossRef]
21. Lacock, S.; du Plessis, A.A.; Booysen, M.J. Electric Vehicle Drivetrain Efficiency and the Multi-Speed Transmission Question. *World Electr. Veh. J.* **2023**, *14*, 342. [CrossRef]
22. Siddique, M.S.; Ertan, H.B.; Alam, M.S.; Khan, M.U. Investigation of Harmonic Losses to Reduce Rotor Copper Loss in Induction Motors for Traction Applications. *World Electr. Veh. J.* **2025**, *16*, 248. [CrossRef]
23. Madhavan, S.; B, R.D.P.; Konda, Y.R.; Gundabattini, E.; Mystkowski, A.; Palka, R.; Wardach, M.; Prajzendanc, P. Thermal management analyses of induction motor through the combination of air-cooling and an integrated water-cooling system. *Sci. Rep.* **2023**, *13*, 10125. [CrossRef]
24. Zhang, B.; Song, Z.; Liu, S.; Huang, R.; Liu, C. Overview of Integrated Electric Motor Drives: Opportunities and Challenges. *Energies* **2022**, *15*, 8299. [CrossRef]
25. Kolar, J.W.; Friedli, T.; Rodriguez, J.; Wheeler, P.W. Review of Three-Phase PWM AC–AC Converter Topologies. *IEEE Trans. Ind. Electron.* **2011**, *58*, 4988–5006. [CrossRef]
26. Ji, Y.; Yang, Y.; Zhou, J.; Ding, H.; Guo, X.; Padmanaban, S. Control Strategies of Mitigating Dead-time Effect on Power Converters: An Overview. *Electronics* **2019**, *8*, 196. [CrossRef]
27. Attia, H.; Che, H.S.; Freddy, T.K.S.; Elkhateb, A. Mitigating the dead-time effects on harmonics spectrum of inverter waveform by the confined band VSFPWM technique. *Int. J. Power Electron. Drive Syst.* **2021**, *12*, 295. [CrossRef]
28. Horri, N. Experimental results of inverter faults impact on the performances of SPWM and SVPWM control techniques. *Prz. Elektrotechniczny* **2025**, *1*, 119–128. [CrossRef]
29. Colak, I.; Kabalci, E. Developing a novel sinusoidal pulse width modulation (SPWM) technique to eliminate side band harmonics. *Int. J. Electr. Power Energy Syst.* **2013**, *44*, 861–871. [CrossRef]
30. Sengamalai, U.; Anbazhagan, G.; Thentral, T.M.T.; Vishnuram, P.; Khurshaid, T.; Kamel, S. Three Phase Induction Motor Drive: A Systematic Review on Dynamic Modeling, Parameter Estimation, and Control Schemes. *Energies* **2022**, *15*, 8260. [CrossRef]
31. Krenicky, T.; Nikitin, Y.; Božek, P. Model-Based Design of Induction Motor Control System in MATLAB. *Appl. Sci.* **2022**, *12*, 11957. [CrossRef]
32. Le Roux, P.F.; Ngwenyama, M.K. Static and Dynamic Simulation of an Induction Motor Using Matlab/Simulink. *Energies* **2022**, *15*, 3564. [CrossRef]

33. Rodriguez-Blanco, M.A.; Golikov, V.; Osorio-Sánchez, R.; Samovarov, O.; Ortiz-Torres, G.; Sanchez-Lara, R.; Vazquez-Avila, J.L. Fault Diagnosis of Induction Motor Using D-Q Simplified Model and Parity Equations. *Energies* **2022**, *15*, 8372. [CrossRef]
34. Reusser, C.A.; Parra, M.; Mino-Aguilar, G.; Gonzalez-Diaz, V.R. Comparison of Induction Machine Drive Control Schemes on the Distribution of Power Losses in a Three-Level NPC Converter. *Machines* **2025**, *13*, 227. [CrossRef]
35. Levron, Y.; Belikov, J.; Baimel, D. A Tutorial on Dynamics and Control of Power Systems with Distributed and Renewable Energy Sources Based on the DQ0 Transformation. *Appl. Sci.* **2018**, *8*, 1661. [CrossRef]
36. Riad, N.; Anis, W.; Elkassas, A.; Hassan, A.E.-W. Three-Phase Multilevel Inverter Using Selective Harmonic Elimination with Marine Predator Algorithm. *Electronics* **2021**, *10*, 374. [CrossRef]

Disclaimer/Publisher's Note: The statements, opinions and data contained in all publications are solely those of the individual author(s) and contributor(s) and not of MDPI and/or the editor(s). MDPI and/or the editor(s) disclaim responsibility for any injury to people or property resulting from any ideas, methods, instructions or products referred to in the content.